

Supercontinuum of a 3.9- μm filament in air: Formation of a two-octave plateau and nonlinearly enhanced linear absorption

Nikolay A. Panov,¹ Daniil E. Shipilo,² Vera A. Andreeva,² Olga G. Kosareva,^{2,*} Alexander M. Saletsky,² Huailiang Xu,³ and Pavel Polynkin⁴

¹*International Laser Center, Lomonosov Moscow State University, 119991 Leninskiye gori 1/62, Moscow, Russia*

²*Faculty of Physics, Lomonosov Moscow State University, 119991 Leninskiye gori 1/2, Moscow, Russia*

³*College of Electronic Science and Engineering, Jilin University, Changchun 130012, China*

⁴*College of Optical Sciences, University of Arizona, Tucson, Arizona 85721, USA*

(Received 10 July 2016; published 6 October 2016)

Through numerical simulations we reveal the scenario of 3.9- μm filament spectrum enrichment in the atmosphere in the cases of linear and circular polarization of the incident pulse. The discrete spectrum of odd harmonics transforms into the two-octave plateau in the case of linear polarization. In contrast, in the case of circular polarization of the incident pulse, the harmonic-free flat supercontinuum appears with the plasma onset, reaching the tenth harmonic of the input radiation. We identify the energy balance specific to the filamentation near 4 μm : the absorption on CO_2 lines in the atmosphere is accelerated by the self-phase modulation in the Kerr nonlinearity early before the plasma channel is formed. This nonlinearly enhanced linear absorption overwhelms the plasma losses and conversion of the input pulse energy to the higher harmonics as well as the plateau.

DOI: [10.1103/PhysRevA.94.041801](https://doi.org/10.1103/PhysRevA.94.041801)

I. INTRODUCTION

Filamentation in transparent medium is accompanied with supercontinuum [1] and third-harmonic generation [2,3]. The broadening of the fundamental radiation under filamentation of an 800-nm radiation spectrum can overlap the whole visible range and reach the third harmonic of input pulse [4]. During past years, the powerful sources (based on optical parametric chirped-pulse amplification [5] mostly) of femtosecond midinfrared radiation (2–4 μm) were developed. The growth of the pulse energy allowed one to observe nonlinear effects in the air under atmospheric pressure. So, experiments [6] show laser amplification of the fifth harmonic of a 1.9- μm femtosecond pulse in the ionized nitrogen N_2^+ . The generation of odd harmonics from a 3.9- μm femtosecond pulse (96 fs, up to 12 mJ) in collimated geometry was observed in air [7]. The spectra were recorded through several-meter propagation in air and revealed the third and fifth harmonics energy oscillations. The period of third-harmonic energy oscillations was ~ 1.5 m, in good agreement with the performed phase-matching analysis. The generation of the higher harmonics up to the 15th was observed in ~ 10 -cm filament in the focusing geometry [8,9]. These harmonics were strongly modulated and spectrally broadened. The main fundamental conclusion from the experiments and simulations [7–9] is that the spectrum of 3.9- μm filament is greatly enriched with the higher-order harmonic components as compared with the 800-nm one.

The theoretical investigation of 3–4 μm filamentation in air revealed the light bullet formation due to anomalous dispersion [10,11]. Other works, aimed at the higher frequency conversion, reported the formation of the plateau in the filament supercontinuum, spanning from the second to the eighth harmonics of 2- μm pump [12,13]. Let us note that Ref. [12] used a quantum-mechanical approach to describe

the nonlinear response of the media; nevertheless, the phenomenological approach [13] gives close results. Moreover, the high frequency continuum generation is proposed as the new mechanism of collapse arrest in 3.9- μm filament [14]. In the papers [12–14], the notable modulation of the plateau is presented as well.

Filamentation of 3.9- μm radiation is characterized by the proximity of a CO_2 absorption band at 4.3 μm . The influence of absorption in this band *per se* on the filamentation and supercontinuum generation by 3.9- μm femtosecond pulses is not studied.

So far, all the cited experiments and simulations involved the linearly polarized radiation. Circular polarization cannot be easily achieved for high-power radiation and requires higher peak power to ensure self-focusing. Therefore, the experimental works with the circularly polarized pulses are quite rare. However, the circular polarization is stable inside the filament [15–17]. Filamentation of circularly polarized pulses provides the spectral broadening comparable to the linear polarization case [18] and helps to stabilize multiple filamentation [19] as well as the terahertz yield [20]. The harmonics generation in isotropic medium is forbidden for circularly polarized radiation. Therefore, the spectral broadening of a circularly polarized 3.9- μm pulse should differ essentially from the linear polarization case. This midinfrared filamentation regime has not been investigated yet.

In this work we investigate numerically the supercontinuum generation and laser-matter energy balance under filamentation of the linearly and circularly polarized 3.9- μm femtosecond pulses on the 7–10-m path in atmospheric air. We reveal the scenarios of spectral broadening in the case of linear and circular polarization and compare them with each other. If the midinfrared pulse is circularly polarized, filamentation leads to the flat nonmodulated plateau in the spectrum spanning over two octaves. The spectral broadening due to filamentation of a 3.9- μm pulse boosts the laser energy absorption by a CO_2 gas band at 4.3 μm . This energy deposition into the medium is

*Corresponding author: kosareva@physics.msu.ru

larger than plasma losses and conversion to supercontinuum. Indeed, this is the nonlinearly enhanced linear absorption in the atmosphere.

II. MODEL

The dynamics of multifrequency filamentation has been studied numerically using a system of coupled equations for harmonics envelopes [3,21]. However, this simulation technique requires clear separation of harmonics' spectra. For the multioctave continuum generation one should use a unified approach which treats all the frequencies in one self-consistent equation. Such approach is realized in a unidirectional pulse propagation equation (UPPE) [22] in the most general form. Forward Maxwell equation (FME) [23] is a paraxial form of a UPPE. Since we study the free propagation of a midinfrared beam, FME is the optimal numerical approach. It neglects the nonparaxial effects, associated with high divergence of radiation, as well as the longitudinal field component. These two effects become significant only under tight focusing conditions (numerical aperture of 0.1 or more [24]). The absence of a longitudinal field allows us to consider the axially symmetrical laser field, $\vec{E}(t,x,y,z) \rightarrow \vec{e}_x E_x(t,r,z) + \vec{e}_y E_y(t,r,z)$, where $r = \sqrt{x^2 + y^2}$ and z is the propagation coordinate.

In FME simulations the carrier wave is resolved and the field components E_x and E_y are real. So a complex-valued function

$$\mathcal{E}(t,r,z) = E_x(t,r,z) + iE_y(t,r,z) \quad (1)$$

allows us to describe arbitrarily polarized radiation without any loss of a phase since we can return to the fields through the transforms $E_x = (\mathcal{E} + \mathcal{E}^*)/2$, $E_y = -i(\mathcal{E} - \mathcal{E}^*)/2$. Then we represent $\mathcal{E}(t,r,z)$ as a composition of Fourier harmonics $\hat{\mathcal{E}}(\omega,r,z)$,

$$\mathcal{E}(t,r,z) = \int_{-\infty}^{+\infty} \hat{\mathcal{E}}(\omega,r,z) \exp(i\omega t) d\omega, \quad (2)$$

where ω is angular frequency. The evolution of harmonics $\hat{\mathcal{E}}(\omega,r,z)$ obeys the equation

$$\frac{\partial \hat{\mathcal{E}}}{\partial z} = -i \left(k(\omega) + \frac{\Delta_{\perp}}{2k(\omega)} \right) \hat{\mathcal{E}} - \frac{2\pi}{c} \hat{\mathcal{J}}, \quad (3)$$

which can be derived from FME. The terms of FME and Eq. (3) are the same, so such representation allows us to easily adapt our FME solver [25] for the case of arbitrary polarization. Denominations in Eq. (3) follow: $k(\omega) = \omega n(\omega)/c$ is a complex-valued wave number, $n(\omega) = n'(\omega) + in''(\omega)$ is a complex index of linear refraction, n' and n'' are refractive and absorption indices, c is a speed of light, $\Delta_{\perp} = r^{-1} \partial/\partial r (r \partial/\partial r \bullet)$ is the transverse Laplacian, and $\hat{\mathcal{J}}(\omega,r,z)$ is related to the material current $\vec{J}(t,r,z)$ through the transforms (1), (2).

We introduce absorption in our simulations since air has relatively strong absorption bands in the vicinity of 4.3 and 6 μm (70 and 50 THz), which are quite close to the central wavelength $\lambda_0 = 3.9 \mu\text{m}$ (76 THz) [see Fig. 1(a)]. These absorption bands correspond to the vibrational excitations of CO_2 and H_2O molecules. The absorption index $n''(\omega)$ is

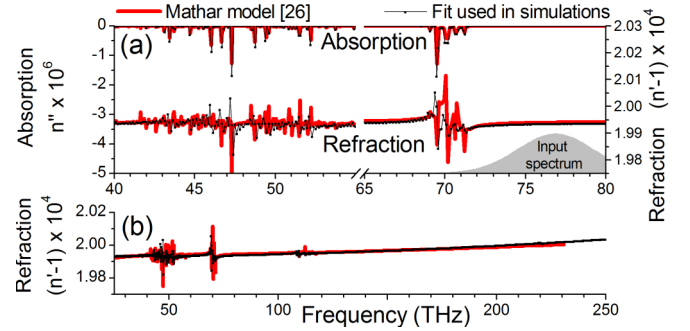


FIG. 1. (a) Absorption and refractive indices in Mathar model [26] [red (gray) lines] and our simulations (black lines); input pulse spectrum (gray area). (b) Overall parabolic dependence of refractive index in the mid- and near infrared.

obtained from Mathar approximation [26] for HITRAN data (temperature 290 K, humidity 10%, CO_2 density 0.04%) and provides the refractive one, $n'(\omega)$, through a pair of direct and inverse Fourier transforms \mathcal{F} and \mathcal{F}^{-1} :

$$n'(\omega) = 1 + A + B\omega^2 + \mathcal{F}[\text{sgn}(t)\mathcal{F}^{-1}[in''(\omega)]], \quad (4)$$

where the last term on the right-hand side serves to satisfy the Kramers-Krönig relations, while the others ($A = 1.993 \times 10^{-4}$, $B = 5.58 \times 10^{-7} \text{ fs}^2$) comply with the parabolic dependence [Fig. 1(b)]. The absorption index is interpolated on our frequency grid with the resolution of ~ 0.1 THz, and Fourier transforms are performed numerically, so that our refractive index does not match the Mathar model perfectly (Fig. 1). It is critical for the simulations to satisfy the Kramers-Krönig relations instead of matching the Mathar refractive index so as to avoid unphysical behavior of the radiation within absorption bands.

The last term in Eq. (4) can be derived as follows. The linear susceptibility $\chi(t)$ is a real function in the temporal domain. Therefore, $2 \text{Re } \hat{\chi}(\omega) = \mathcal{F}[\chi(t) + \chi(-t)]$ and $2i \text{Im } \hat{\chi}(\omega) = \mathcal{F}[\chi(t) - \chi(-t)]$, where $\hat{\chi}(\omega)$ is the representation of $\chi(t)$ in the Fourier domain. The Kramers-Krönig relations can be written in the temporal domain as $\chi(t < 0) = 0$, hence $[\chi(t) + \chi(-t)] = \text{sgn}(t)[\chi(t) - \chi(-t)]$. So, $\text{Re } \hat{\chi}(\omega) = \mathcal{F}[\text{sgn}(t)\mathcal{F}^{-1}[i \text{Im } \hat{\chi}(\omega)]]$, which corresponds to the last term in Eq. (4).

Material current $J(t,r,z) = \partial \vec{P}/\partial t + \vec{J}_{\text{abs}} + \vec{J}_{\text{free}}$ describes nonlinear effects and is determined from the electric field $\vec{E}(t,r,z)$. The equation for nonlinear polarization $\vec{P}(t) = \chi^{(3)}|\vec{E}(t)|^2 \vec{E}(t)$ in the case of arbitrarily polarized field is given in [27]. The third-order susceptibility $\chi^{(3)}$ corresponds to the nonlinear refractive index of $10^{-19} \text{ cm}^2/\text{W}$. We include the fast electronic Kerr response only. The nonlinear excitations of molecular rotations have the 70-fs delayed response [28] and cannot change the generation of harmonics and ultrabroad supercontinuum, which is governed by the intraperiod processes. Inside the filament the energy transmitted into rotations is about 0.004 eV/molecule [29], and, assuming a factor of 10^3 - 10^4 exceed of neutrals over the free electrons, might reach the level of ionization loss. Thus, the decisive impact on the spectrum comes from the fast electronic response, while the slower molecular response does not have the dominating effect on the absorption either.

The equations for absorption and free electron currents \vec{J}_{abs} and \vec{J}_{free} , respectively, for arbitrarily polarized radiation are quite the same as in the case of the linearly polarized one (see, e.g., [25]). Such equations include the intraperiod ionization, the generation of Brunel harmonics [30], and self-phase modulation. We choose the electron-neutral collision frequency $\nu_c = 5 \text{ ps}^{-1}$. We checked that the increase of this value up to 25 ps^{-1} influences the results of the paper insignificantly.

The ionization is described in the tunneling regime as the Keldysh parameter γ for 3.9 μm radiation is much less than unity for intensities of $40 \text{ TW}/\text{cm}^2$ and higher. Free electron density $N_e(t)$ is obtained from equation $\partial N_e(t)/\partial t = w(|\vec{E}(t)|)[N_0 - N_e(t)]$, where N_0 is a neutral gas density, $w(E)$ is a rate of ionization [31–33]:

$$w(E) = 4 \omega_{\text{at}} r_{\text{H}}^{2.5} \frac{E_{\text{at}}}{E} \exp\left(-\frac{2}{3} r_{\text{H}}^{1.5} \frac{E_{\text{at}}}{E}\right), \quad (5)$$

$\omega_{\text{at}} = 41.3 \text{ fs}^{-1}$ is the atomic frequency unit, $E_{\text{at}} = 5.17 \text{ GV}/\text{cm}$ is the atomic electric field strength, and $r_{\text{H}} = U_i/U_{\text{H}}$ is the ratio between the ionization potentials of neutrals to be ionized and a hydrogen atom. For the purpose of free electron generation we assume that air consists of oxygen and nitrogen only. The influence of the ellipticity ξ of the field polarization ($|\xi| \leq 1$) on the ionization rate is described [31] as $\ln w(E) \sim (-\frac{2}{3} r_{\text{H}}^{1.5} \frac{E_{\text{at}}}{E} [1 - (1 - \frac{\xi^2}{3}) \frac{\nu_c^2}{10}])$. Since we neglect the $\propto \gamma^2$ terms, Eq. (5) describes the ionization by circularly polarized radiation satisfactorily.

We neglect the avalanche ionization for the following reason: the ponderomotive energy for an intensity of $\sim 100 \text{ TW}/\text{cm}^2$ and a frequency of 76 THz can reach 100 eV , so every electron-neutral collision will release a new electron. But the provided avalanche addition to the ionization rate $\nu_c N_e$ is much less than $w(E)N_0$ since $N_e \ll N_0$ and $\nu_c \lesssim w(E)$.

We study the filamentation of linearly and circularly polarized pulses. The initial conditions read:

$$\begin{aligned} \mathcal{E}(t, r, z = 0) = E_0 \exp\left(-\frac{r^2}{2a_0^2} - \frac{t^2}{2\tau_0^2}\right) \\ \times \begin{cases} \cos(\omega_0 t) & \text{for linear polarization} \\ \frac{1}{\sqrt{2}} \exp(i\omega_0 t) & \text{for circular polarization,} \end{cases} \end{aligned} \quad (6)$$

where E_0 is a field amplitude corresponding to a total energy of the pulse W_0 , a beam diameter $2a_0$, and a pulse duration $2\tau_0 = 96 \text{ fs}$; $\omega_0 = 2\pi c/\lambda_0$ is a laser frequency.

III. RESULTS

A. Harmonics generation below filamentation threshold

First we investigate the spectral enrichment of the 3.9- μm linearly polarized femtosecond radiation in the experimental conditions [7] so as to obtain a reference for the further study: $W_0 = 12 \text{ mJ}$ and $2a_0 = 1.2 \text{ cm}$. The filamentation does not occur for such a pulse since its peak power is about half of the critical power for self-focusing. Besides, the wing of the input radiation spectrum overlaps with the CO_2 absorption band near

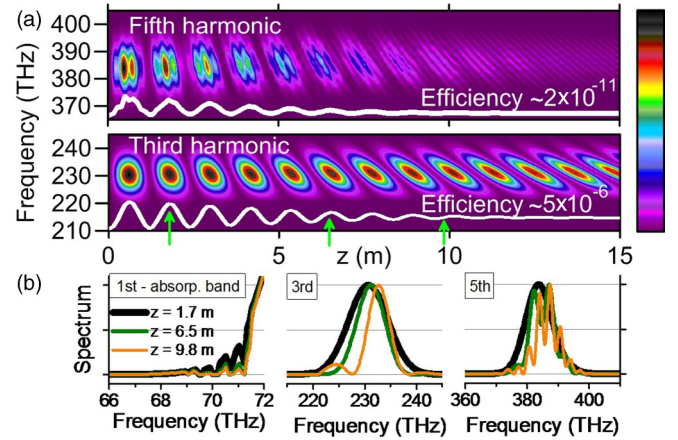


FIG. 2. (a) Third and fifth harmonics spectra evolution with propagation distance for a 12-mJ pulse. Each harmonic has its own linear color scale. White curves indicate conversion efficiency (i.e., the spectrum integrated over a 200–250 THz or 360–410 THz range). (b) Normalized spectra of harmonics at several distances, marked with the arrows in panel (a).

70 THz [Figs. 1(a), 2(b)]. The resulting energy loss is about 1% of the input pulse energy at $z = 15 \text{ m}$.

Despite the nonfilamenting regime and absorption, the odd harmonics are well pronounced (Fig. 2). The phase mismatch limits the energy of harmonics. The conversion efficiencies of the third and fifth harmonics are $\sim 10^{-5}$ and $\sim 10^{-11}$, respectively. The seventh and higher harmonics have the energy below 100 of photons and they have not been observed in the experiment [7]. The third-harmonic energy follows the expression $W_{3\omega_0}(z) \propto \sin^2(\frac{1}{2}[k(3\omega_0) - 3k(\omega_0)]z) = \sin^2(\pi z/[160 \text{ cm}])$, which is obtained for continuous plane-wave and material dispersion [26]. The fifth harmonic is generated in the cascade process and has additional modulation at spatial frequency $[k(5\omega_0) - k(3\omega_0) - 2k(\omega_0)] = 2\pi/(41 \text{ cm})$. The conversion efficiency oscillates and the separated bulbs appear along the propagation. Exactly this effect was observed experimentally and calculated under the assumption of the higher-order Kerr effect (HOKE) in Ref. [7]. The higher-order susceptibilities were adjusted there for the best fit of the experimental data. However, the chosen values correspond to the relation $n_4 I^2/(n_2 I) = 0.4$, for the intensity $I = 0.2 \text{ TW}/\text{cm}^2$ [cf. with $n_4 I^2/(n_2 I) = 0.0025$ for the same intensity according to [34]]. This value seems to be too large for the perturbative approach which implies the successive term to be much smaller than the preceding term (Ref. [35]). We have not included HOKE into our simulations after checking that for the fifth-order susceptibility measured in [34] the direct mechanism of harmonic generation is negligible as compared with the cascade one.

The oscillations of harmonics energy vanish and the conversion efficiency reaches almost the constant value as soon as the tilt of the bulbs in the propagation-resolved spectrum becomes pronounced [Fig. 2(a)]. This tilt is associated with the harmonic pulse splitting in temporal domain due to the continuous process of harmonic generation, back conversion, and group velocity walk-off [Figs. 3(a)–3(f)]. One portion of the harmonic pulse is locked within the fundamental pulse and

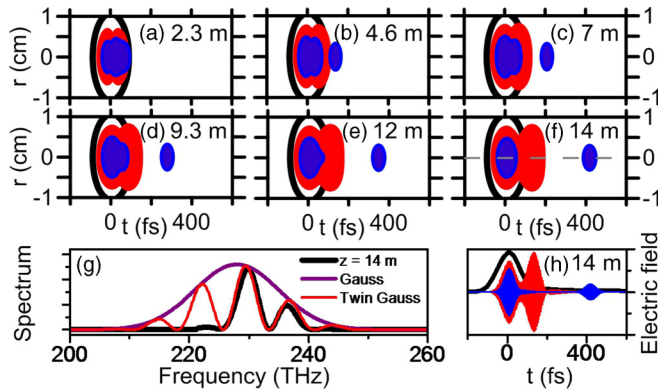


FIG. 3. (a)–(f) Spatiotemporal distributions of the fundamental radiation (black contour), the third harmonic [red (light-gray) filled contour], and the fifth harmonic [blue (dark-gray) filled contour] for a 12-mJ pulse. (g) Third-harmonic spectrum at $z = 14$ m, where two third-harmonic subpulses are 125 fs away from each other, and the spectrum $S_{\text{twin}}(\omega)$. (h) Normalized time-dependent envelope of the first harmonic (black curve), field of the third and the fifth harmonics [red (light-gray) and blue (dark-gray) curves, respectively] on the beam axis at $z = 14$ m.

its energy is stabilized in the ongoing nonlinear interaction with the pump [3,36]; the other portion exits the interaction zone and is not fed by the pump any longer. The resulting energy converted into the range 200–250 THz for the third harmonic or 360–410 THz for the fifth harmonic remains constant with further propagation. At a particular frequency the spectral intensity continues to oscillate [e.g., 230 THz in Fig. 2(a)]. The delay τ between the phase-locked and traveled out harmonic pulses, each of which has the power spectrum $S_{\text{harm}}(\omega)$, results in the characteristic spectrum with modulations $S_{\text{twin}}(\omega) = 2(1 + \cos \omega\tau)S_{\text{harm}}(\omega)$ [Figs. 3(f) and 3(h)]. For a 2- μm driver in solids this effect was observed in [37].

B. Filamentation regime: Spectral plateau and energy balance

Now we increase the energy of the pulse up to $W_0 = 80$ mJ so as to reach the filamentation threshold for both the linearly and circularly polarized pulses. Also we decrease the beam diameter to $2a_0 = 0.6$ cm to avoid the intensity drop due to dispersive broadening. For the linearly polarized input pulse, the evolution of the spectrum with the propagation distance is presented in Fig. 4(a). Odd harmonics behave similarly to their counterparts in the low-energy pulse (Fig. 2). Starting from where the plasma channel is established, the quick broadening of the spectrum occurs. The Brunel harmonics are generated as well; however, their clear identification is difficult since their generation and the plasma-induced spectral broadening develop simultaneously. Discreteness of harmonics transforms to supercontinuum from 50 to 900 THz [Fig. 4(a), $z > 5$ m]. A quasiplateau spans from ~ 150 to ~ 550 THz [from second to eighth harmonic; see Fig. 4(c), blue (dark-gray) line]. The plateau is strongly modulated due to simultaneous generation of harmonics and broadening of the spectrum. The angular structure of the radiation in our conditions of collimated propagation does not show the characteristic conical rings

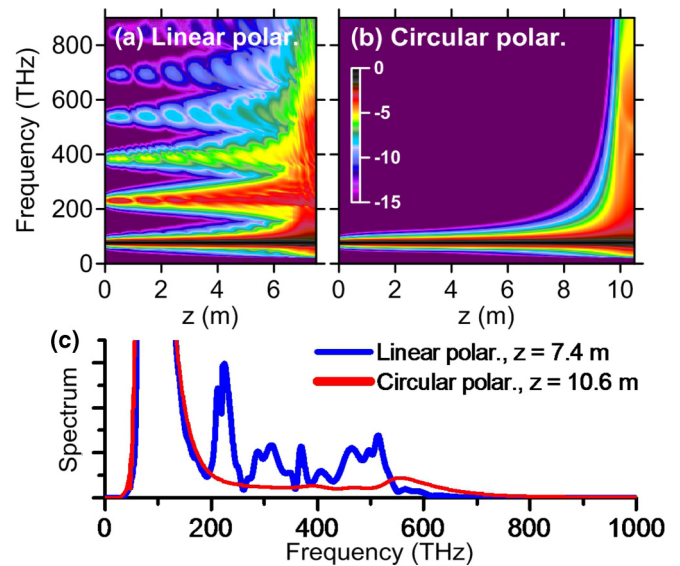


FIG. 4. Evolution with the propagation distance z of the spectra of 80-mJ (a) linearly and (b) circularly polarized pulses (logarithmic color scale). (c) The comparison between the spectra induced by the linearly [blue (dark-gray) curve] and circularly [red (light-gray) curve] polarized pulses.

either from the fundamental radiation [1] (due to the weak anomalous dispersion [38]) or from harmonics [8,9]. We associate the conical structure of harmonics from the 3.9- μm filament reported in Refs. [8,9] with the higher plasma density induced by geometrical focusing of the beam.

So far, we would like to clearly pronounce the three stages of supercontinuum generation in the linearly polarized 3.9- μm filament: (i) the separated optical harmonics, up to the ninth one, appear from a cascade mechanism with energies oscillating due to the phase mismatch; (ii) group velocity walk-off leads to the formation of a twin-pulse structure of harmonics in the temporal domain, so that their spectra become strongly modulated and their efficiency saturates; (iii) the spectral broadening of each harmonic in the developed filament provides the strongly modulated quasiplateau supercontinuum.

This scenario of higher-order harmonic to extended plateau generation is in contrast with supercontinuum generation in a 800-nm filament, for which the spectrum extends until the third harmonic only [4], the latter being locked and not traveling away from the pump [3]. The physics of these contrasting features is that in a 3.9- μm filament the material dispersion is less pronounced than in the 800-nm case. The third (fifth) harmonic of 3.9- μm pump accumulates energy in the favorable conditions of 160 cm (41 cm) coherence length as compared with the 800-nm case (1.4 and 0.3 cm, respectively). Being locked within the fundamental pulse, the higher harmonics are amplified and broadened with the intensity growth. These higher harmonics form the shock wave [14] and the plateau in the developed filament.

In addition to the higher frequency spectral enrichment, the broadening of the fundamental harmonic (76 THz) to the low-frequency range takes place continuously in the propagation. The broadened spectrum reaches 50 THz [Fig. 4(c)] and initiates the new type of absorption. The initial spectrum is

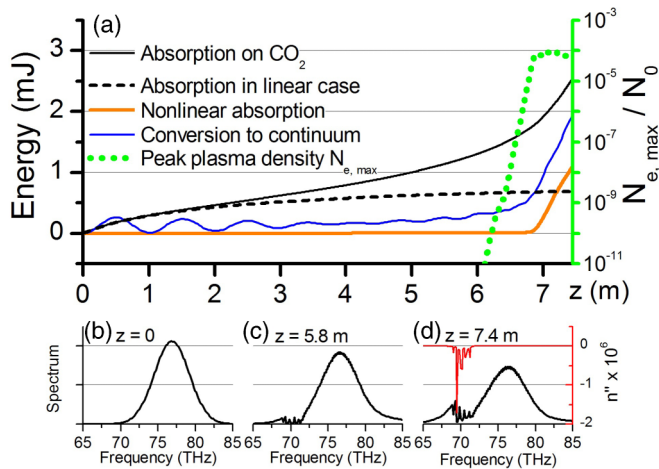


FIG. 5. (a) Deposition of 80-mJ pulse energy into the CO_2 band at 70 THz (black solid curve), high-frequency continuum [150–750 THz, blue (dark-gray) curve], and plasma [both ionization and J_{free} relaxation, orange (light-gray) curve]. Black dashed curve is absorption in the atmosphere in the linear propagation case. Green (light-gray) dotted curve (corresponds to right axis) is peak free electron density. (b)–(d) Spectral broadening over the absorption band at several distances (black lines) and absorption index [red (gray) curve, right axis].

broadened nonlinearly towards the atmospheric CO_2 absorption band and then absorbed by CO_2 . This is a linear absorption enhanced by the strong field in a 3.9- μm 80-mJ filament because of a continuous supply of energy from the pump into this band. Thus, the 3.9- μm filament, unlike the 800-nm one, has an extra channel of loss in the atmosphere.

The energy balance in the filamentation regime is represented by absorption due to plasma, conversion to supercontinuum, and absorption in the atmospheric constituents [Fig. 5(a)]. The higher frequency wing of supercontinuum (from the second to the tenth harmonic) consumes 2.5% of input energy [2 mJ, blue (dark-gray) curve in Fig. 5(a)] by $z = 7.5$ m. The free electron formation and their heating due to collisions leads to the absorption of about 1.3% [1 mJ, orange (light-gray) curve in Fig. 5(a)]. Both supercontinuum and plasma losses are directly associated with the plasma channel establishment ($z \approx 7$ m). On the contrary, the atmospheric absorption on the CO_2 band persists through the whole propagation path, exceeding supercontinuum and plasma losses [cf. black solid curve with blue (dark-gray) and orange (light-gray) ones in Fig. 5(a)]. Nonlinear enhancement of this CO_2 absorption starts at $z \approx 2.5$ m due to spectral broadening on Kerr nonlinearity before the intensity reaches ionization threshold. The total absorbed energy due to CO_2 is more than 3% (2.5 mJ out of input 80 mJ). This type of absorption is successively revealed in the spectrum with the propagation distance [Figs. 5(b)–5(d)]. Thus, we clearly demonstrate the new absorption mechanism—nonlinearly enhanced linear absorption, which should not be neglected under filamentation of 3.9- μm radiation.

C. Circularly polarized pulse

The generation of optical harmonics is forbidden for the case of a circularly polarized pulse [39]. Hence the first two stages of the previous scenario are not reproduced: the spectrum is not enriched with harmonics but only broadened slightly [Fig. 4(b), $z < 8$ m]. As soon as the ionization threshold is reached, the rapid growth of plasma density within a fraction of the pulse duration together with the formed shock wave provide the ultrabroad spectrum which reaches almost the same frequency range as in the previous case [50–800 THz, red (light-gray) line in Fig. 4(c)]. The comparison between the supercontinuum spectra of the linearly and circularly polarized pulses reveals that the circularly polarized light produces the flat plateau spanning over two octaves (150–600 THz). The abrupt cut-off of the spectra, best seen for the linearly polarized case, was investigated both numerically and experimentally in solids for the wide range of incident frequencies [40–42] and explained via interference effects [38].

The low-frequency spectral broadening of the circularly polarized pulse is similar to that of the linearly polarized pulse. Hence, the nonlinearly enhanced linear absorption is the same as in the previous case. The plasma losses are slightly less than in the linear polarization case. The conversion to the higher frequency wing of supercontinuum is several times lower than for the linear polarization case, which is best seen in Fig. 4(c).

IV. CONCLUSION

We reveal the scenario of 3.9- μm filament spectrum enrichment in the cases of linear and circular polarization of the input pulse. The discrete spectrum of odd harmonics transforms to the two-octave plateau in the case of linear polarization. This transformation occurs through harmonic walk-off, split harmonic pulse formation, and resulting spectral modulation with the extreme broadening in the plasma filament. In contrast, in the case of circular polarization of the input pulse, the harmonic-free flat supercontinuum appears with the plasma onset reaching the tenth harmonic of 3.9- μm radiation.

The supercontinuum generation is closely connected to the unusual energy balance in the midinfrared filament. The linear absorption on CO_2 lines is accelerated by the self-phase modulation in the Kerr nonlinearity before the plasma channel is formed. This absorption overwhelms the nonlinear ones due to the plasma loss and conversion to the harmonics and extended plateau. Thus, we clearly demonstrate the specific absorption mechanism, which cannot be neglected under filamentation of 3.9- μm radiation in the atmosphere—nonlinearly enhanced linear absorption.

ACKNOWLEDGMENTS

All of the authors acknowledge essential contributions from Professor See Leang Chin who provided us with advice, constructive criticism, and fruitful discussions. N.A.P., D.E.S., V.A.A., and O.G.K. acknowledge the support from Russian Science Foundation (Grant No. 16-42-01060). P.P. acknowledges the support from the U.S. Air Force Office of Scientific Research under MURI award No. FA9550-16-1-0013 and from the U.S. Defense Threat Reduction Agency under program No. HDTRA 1-14-1-0009.

- [1] V. P. Kandidov, O. G. Kosareva, I. S. Golubtsov, W. Liu, A. Becker, N. Akozbek, C. M. Bowden, and S. L. Chin, *Appl. Phys. B* **77**, 149 (2003).
- [2] A. B. Fedotov, N. I. Koroteev, M. Loy, X. Xiao, and A. M. Zheltikov, *Opt. Commun.* **133**, 587 (1997).
- [3] N. Aközbeke, A. Iwasaki, A. Becker, M. Scalora, S. L. Chin, and C. M. Bowden, *Phys. Rev. Lett.* **89**, 143901 (2002).
- [4] F. Theberge, W. Liu, Q. Luo, and S. L. Chin, *Appl. Phys. B* **80**, 221 (2005).
- [5] R. Butkus, R. Danielius, A. Dubietis, A. Piskarskas, and A. Stabinis, *Appl. Phys. B* **79**, 693 (2004).
- [6] J. Yao, B. Zeng, H. Xu, G. Li, W. Chu, J. Ni, H. Zhang, S. L. Chin, Y. Cheng, and Z. Xu, *Phys. Rev. A* **84**, 051802 (2011).
- [7] D. Kartashov, S. Ališauskas, A. Pugžlys, A. A. Voronin, A. M. Zheltikov, and A. Baltuška, *Opt. Lett.* **37**, 2268 (2012).
- [8] A. V. Mitrofanov *et al.*, *Opt. Lett.* **40**, 2068 (2015).
- [9] A. V. Mitrofanov *et al.*, *Sci. Rep.* **5**, 8368 (2015).
- [10] B. Shim, S. E. Schrauth, and A. L. Gaeta, *Opt. Express* **19**, 9118 (2011).
- [11] S. V. Chekalin, A. E. Dokukina, A. E. Dormidonov, V. O. Kompanets, E. O. Smetanina, and V. P. Kandidov, *J. Phys. B* **48**, 094008 (2015).
- [12] M. Kolesik, J. M. Brown, A. Teleki, P. Jakobsen, J. V. Moloney, and E. M. Wright, *Optica* **1**, 323 (2014).
- [13] L. Bergé, C.-L. Soulez, C. Köhler, and S. Skupin, *Appl. Phys. B* **103**, 563 (2011).
- [14] P. Panagiotopoulos, P. Whalen, M. Kolesik, and J. V. Moloney, *Nat. Photonics* **9**, 543 (2015).
- [15] M. Kolesik, J. V. Moloney, and E. M. Wright, *Phys. Rev. E* **64**, 046607 (2001).
- [16] N. A. Panov, O. G. Kosareva, A. B. Savel'ev, D. S. Uryupina, I. A. Perezhogin, and V. A. Makarov, *Quantum Electron.* **41**, 160 (2011).
- [17] N. A. Panov, V. A. Makarov, V. Y. Fedorov, and O. G. Kosareva, *Opt. Lett.* **38**, 537 (2013).
- [18] H. Yang *et al.*, *Opt. Lett.* **30**, 534 (2005).
- [19] A. Trisorio and C. P. Hauri, *Opt. Lett.* **32**, 1650 (2007).
- [20] M. Esaulkov, O. Kosareva, V. Makarov, N. Panov, and A. Shkurinov, *Frontiers Optoelectron.* **8**, 73 (2015).
- [21] O. Kosareva *et al.*, *Opt. Lett.* **35**, 2904 (2010).
- [22] M. Kolesik and J. V. Moloney, *Phys. Rev. E* **70**, 036604 (2004).
- [23] A. V. Husakou and J. Herrmann, *Phys. Rev. Lett.* **87**, 203901 (2001).
- [24] A. Couairon, O. G. Kosareva, N. A. Panov, D. E. Shipilo, V. A. Andreeva, V. Jukna, and F. Nesa, *Opt. Express* **23**, 31240 (2015).
- [25] N. A. Panov, D. E. Shipilo, V. A. Andreeva, D. S. Uryupina, A. B. Savel'ev, O. G. Kosareva, and S. L. Chin, *Appl. Phys. B* **120**, 383 (2015).
- [26] R. J. Mathar, *Appl. Opt.* **43**, 928 (2004).
- [27] A. V. Borodin *et al.*, *Opt. Lett.* **38**, 1906 (2013).
- [28] E. Nibbering, G. Grillon, M. A. Franco, B. S. Prade, and A. Mysyrowicz, *J. Opt. Soc. Am. B* **14**, 650 (1997).
- [29] J. K. Wahlstrand, N. Jhaji, E. W. Rosenthal, S. Zahedpour, and H. M. Milchberg, *Opt. Lett.* **39**, 1290 (2014).
- [30] F. Brunel, *J. Opt. Soc. Am. B* **7**, 521 (1990).
- [31] V. S. Popov, *Sov. Phys. Usp.* **47**, 855 (2004).
- [32] L. D. Landau and E. M. Lifshitz, *Quantum Mechanics* (Pergamon, New York, 1965).
- [33] M. D. Thomson, M. Kreß, T. Löffler, and H. G. Roskos, *Laser Photonics Rev.* **1**, 349 (2007).
- [34] V. Loriot, E. Hertz, O. Faucher, and B. Lavorel, *Opt. Express* **18**, 3011 (2010).
- [35] E. A. Volkova, A. M. Popov, and O. V. Tikhonova, *Quantum Electron.* **42**, 680 (2012).
- [36] V. Roppo *et al.*, *Phys. Rev. A* **76**, 033829 (2007).
- [37] N. Garejev, I. Gražulevičiūtė, D. Majus, G. Tamošauskas, V. Jukna, A. Couairon, and A. Dubietis, *Phys. Rev. A* **89**, 033846 (2014).
- [38] A. E. Dormidonov and V. P. Kandidov, *Laser Phys.* **19**, 1993 (2009).
- [39] Y. R. Shen, *Principles of Nonlinear Optics* (Wiley, New York, 1984).
- [40] E. O. Smetanina, V. O. Kompanets, S. V. Chekalin, and V. P. Kandidov, *Quantum Electron.* **42**, 913 (2012).
- [41] E. O. Smetanina, V. O. Kompanets, S. V. Chekalin, and V. P. Kandidov, *Quantum Electron.* **42**, 920 (2012).
- [42] E. O. Smetanina, V. O. Kompanets, S. V. Chekalin, A. E. Dormidonov, and V. P. Kandidov, *Opt. Lett.* **38**, 16 (2013).